ACS SENSORS

pubs.acs.org/acssensors

Letter

Colorimetric Test for Fast Detection of SARS-CoV-2 in Nasal and Throat Swabs

Bartolomeo Della Ventura, Michele Cennamo, Antonio Minopoli, Raffaele Campanile, Sergio Bolletti Censi, Daniela Terracciano, Giuseppe Portella,* and Raffaele Velotta*

Cite This: https://dx.doi.org/10.1021/acssensors.0c01742

Read Online

ACCESS | Metrics & More | Article Recommendations | Supporting Information

ABSTRACT: Mass testing is fundamental to face the pandemic caused by the coronavirus SARS-CoV-2 discovered at the end of 2019. To this aim, it is necessary to establish reliable, fast, and cheap tools to detect viral particles in biological material so to identify the people capable of spreading the infection. We demonstrate that a colorimetric biosensor based on gold nanoparticle (AuNP) interaction induced by SARS-CoV-2 lends itself as an outstanding tool for detecting viral particles in nasal and throat swabs. The extinction spectrum of a colloidal solution of multiple viral-target gold nanoparticles—AuNPs functionalized with antibodies targeting three surface proteins of SARS-CoV-2 (spike, envelope, and membrane)—is red-shifted in few minutes when mixed with a solution containing the viral particle. The optical density of the mixed solution measured at 560 nm was compared to the threshold cycle (C_t) of a real-time PCR (gold standard for detecting the presence of viruses) finding that the colorimetric method is able to detect very low viral load with a detection limit approaching that of the real-time PCR. Since the method is sensitive to the infecting viral particle rather than to its RNA, the achievements reported here open a new perspective not only in the context of the current and possible future pandemics, but also in microbiology, as the biosensor proves itself to be a powerful though simple tool for measuring the viral particle concentration.

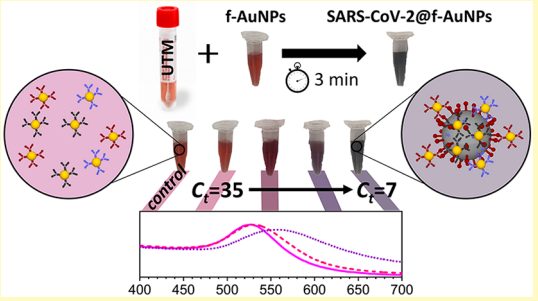

KEYWORDS: *SARS-CoV-2, colorimetric biosensors, point-of-care device, photochemical immobilization technique, antibody, gold nanoparticles*

Since its identification in China in late 2019, the SARS-CoV-2 epidemic has spread rapidly worldwide affecting millions of people, thus pushing the World Health Organization (WHO) to declare a COVID-19 outbreak a global health emergency. Mass testing is fundamental to identify and isolate clusters in order to limit and eventually eradicate SARS-CoV-2.[1] The gold standard for diagnosing COVID-19 infection is a reverse transcription real-time polymerase chain reaction (real-time PCR)[2] that is able to detect the virus genetic material (RNA) in samples collected via nasopharyngeal swab. Currently, only qualitative real-time PCR assays are available that yield positive/negative results without providing information about the viral load. Due to its complexity, real-time PCR tests are performed in certified laboratories, are time-consuming, require experienced personnel, and can hardly lend themselves to mass screening.[3−6] Huge efforts are put into overcoming such a bottleneck, thereby making nucleic acid amplification suitable for point-of-care tests, but the variety of methods[7] and the lack of any commercial solution demonstrates that the gap between research and real applications is still to be filled.[8] The main reason for that has to be found in the detection principle (RNA-extraction, reverse transcription, and amplification) whose complexity, though greatly reduced by several approaches (e.g., loop-mediated isothermal amplification (LAMP) and recombinase polymerase amplification (RPA) or CRISPR-based detection), is far from being used for quick POC tests.

Lateral flow assays (LFA)s are among the actual biosensing platforms for home tests and potentially for mass screening,[9−12] but the relatively poor sensitivity inherent to this technology[13] makes the quest for a different approach urgent.[14] Biosensors based on metal nanoparticles are often proposed because of their unique optical properties, which makes them potentially suitable to develop easy-to-use and rapid colorimetric diagnostic tests for point-of-care applications or even for home use.[15] Due to its surface chemistry and given its biocompatibility, gold is generally preferred to other metals.[16] The physical process underlying this class of biosensors is the

Received: August 20, 2020
Accepted: September 29, 2020
Published: September 29, 2020

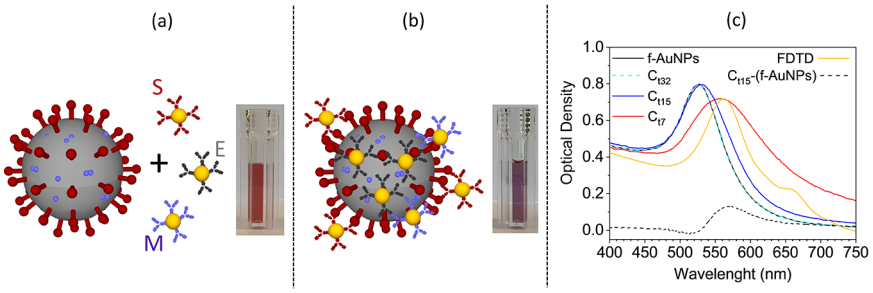

Figure 1. (a) Sketch of the SARS-CoV-2 and functionalized AuNPs. SARS-CoV-2 proteins (spike, membrane, and envelope) and their corresponding antibody (S, E, and M) are highlighted in dark red, light violet, and gray, respectively. The inset shows the pink colloidal solution containing the anti-SARS-CoV-2 functionalized AuNPs (f-AuNPs). (b) The f-AuNPs surround the virion forming a nanoparticle layer on its surface. Their interaction leads to a shift of the resonance peak in the extinction spectrum and, hence, to a color change visible in the inset. (c) Extinction spectra reporting the OD of f-AuNP colloidal solution mixed with samples from patients with different viral load. At very low virion concentration (curve C_{t32}) the extinction spectrum is not distinguishable from the spectrum of f-AuNPs (black continuous line). At intermediate virion concentration (curve C_{t15}) the extinction spectrum is slightly red-shifted and its difference from the "control" (f-AuNPs) produces the curve C_{t15}-(f-AuNPs) that evidences the contribution entailed by the virion. At high virion concentration (curve C_{t7}), the extinction spectrum peaks at 560 nm as for C_{t15}-(f-AuNPs). The agreement between the curve C_7 and the simulated spectrum (gold continuous line, scaled to the experimental one) from a dielectric sphere (100 nm diameter) surrounded by smaller AuNPs (20 nm diameter) confirms the interpretation of the extinction spectra as due to nanoparticle aggregation.

localized surface plasmon resonance (LSPR) that consists of coherent and nonpropagating oscillations of free electrons in metal nanoparticles arising when they interact with an electromagnetic wave whose frequency resonates with the plasmonic one.[17,18] Colorimetric detection based on gold nanoparticles (AuNPs) takes advantage of the color change occurring in a colloidal suspension from red to blue as a result of LSPR coupling among the nanoparticles.[19] AuNP aggregation can be regulated using biological mechanisms such as antigen−antibody (Ab) interaction, in which case different strategies can be used to immobilize Abs correctly oriented on the surface of the AuNPs, although the complexity of the standard procedures makes them unsuitable for industrial applications on a large scale.[20]

The photochemical immobilization technique (PIT) is a surface functionalization procedure that only requires UV activation of the Abs and leads to a high-density functionalized surface within minutes.[21,22] PIT has proven itself to be effective in tethering Abs upright not only on flat surfaces,[23−26] but also on AuNPs, which were used either to ballast small antigen[27] or to realize a colorimetric biosensor for detecting IgGs[28] and estradiol.[29] In the latter cases, the presence of the antigen was detected as a change in the absorbance that can be easily measured by a spectrophotometer or even by naked eye. An approach relying on nanoparticle aggregation induced by the presence of the antigen was also used to detect the influenza A virus, but no clinical application was reported to demonstrate the effectiveness of the whole procedure in clinical cases.[30]

Here, we report on the realization of a colorimetric biosensor that can be used for COVID-19 mass testing with sensitivity and specificity higher that 95% as demonstrated by a comparative analysis carried out on a total of 94 samples (45 positive and 49 negative), tested by standard real-time PCR in the Virology Unit of A.O.U. Federico II/Department of Translational Medicine of the University of Naples "Federico II". The detection scheme is shown in Figure 1a,b and consists of a colloidal solution of PIT-functionalized AuNPs (f-AuNPs) against three surface proteins of SARS-CoV-2: spike, envelope, and membrane (S, E, and M, respectively, in Figure 1a). AuNP fabrication (20 nm diameter), characterization, and functionalization are described in the Supporting Information (see sections S1−S5 and Figures S1−S3 of SI), that contains a scalable procedure to realize the colloidal solution for COVID-19 test. In this approach, the sample was a solution of Universal Transport Medium (UTM, Copan Brescia, Italy), in which the specimen was dipped after its collection from the patient and without any additional treatment (see section S6 of Supporting Information). Our test was carried out by mixing 50 μL of the f-AuNP colloidal solution with 100 μL of sample and 100 μL of ultrapure water. The presence of the viral particles (virions) induced the formation of a nanoparticle layer on its surface (Figure 1b) that led to a redshift of the optical density (OD) in the extinction spectrum of the solution (Figure 1c). When the viral load was relatively high, i.e., C_t < 15 (see section S7 of Supporting Information), the color change from red to purple was visible even by the naked eye (Figure 1a,b).

The extinction spectrum of f-AuNPs reported in Figure 1c (black continuous line) is not distinguishable from the spectrum of a mixed solution with a sample having C_t = 32 (dashed light blue curve, C_{t32}). On the contrary, red shift is observed for a sample with C_t = 15 (blue continuous line, C_{t15}), which becomes much more noticeable when C_t = 7 (red continuous line, C_{t7}). The contribution of the virion (surrounded by nanoparticles) to the extinction spectrum can be deduced by subtracting the spectrum of f-AuNPs from C_{t15}. In fact, the curve C_{t15}-(f-AuNPs) shows a peak at a wavelength comparable to that exhibited by C_{t7} (approximately 560 nm).

To further confirm that the spectrum C_{t7} arose from f-AuNPs surrounding SARS-CoV-2, we simulated the virion as a 100-nm-diameter[31,32] dielectric sphere of 1.45 refractive index.[33] A changeable number of gold nanoparticles (20 nm diameter)[34] were randomly positioned on the sphere (see section S8 of Supporting Information). We implemented the "FDTD solutions" tool in Lumerical software that provides numerical solutions to the Maxwell's equations by the finite-difference time-domain (FDTD) method within a Mie problem-like workspace. A sketch of the simulation workspace is depicted in Figure S4a, whereas Figure S4b shows the LSPR wavelength as a function of the number of AuNPs on the virion surface. The dependence of the plasmon resonance on the

https://dx.doi.org/10.1021/acssensors.0c01742
ACS Sens. XXXX, XXX, XXX−XXX

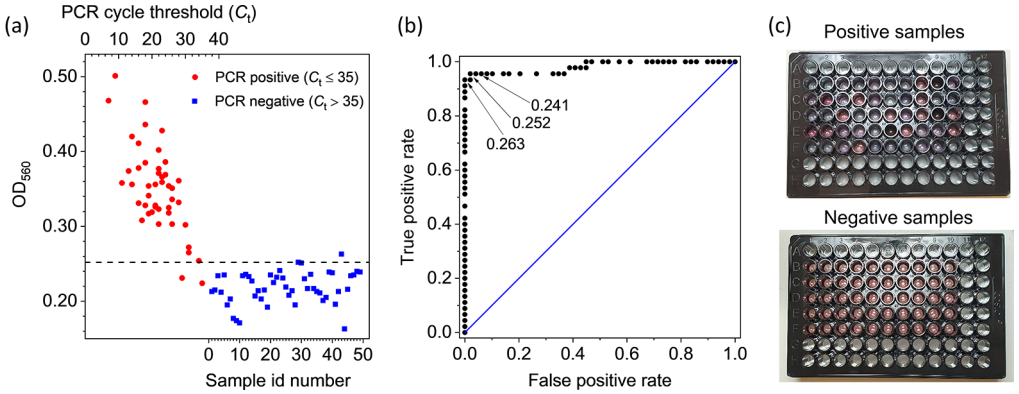

Figure 2. (a) Results of the colorimetric test on real thawed samples from 45 positive (red circle points) and 49 negative patients (blue square points) previously tested by real-time PCR. For all of them, the extinction coefficient was measured at 560 nm. The positive samples ($C_t \leq 35$) are identified in the plot by their real-time PCR cycle threshold (top scale), whereas the negative samples ($C_t > 35$) are simply numbered (bottom scale). The horizontal line at 0.252 extinction coefficient would lead to a test with 96% sensitivity and 98% specificity. (b) ROC curve retrieved from the data of the panel (a). The area under the curve is 0.98. Also shown are three threshold values for the extinction coefficient that would provide the following sensitivity and specificity: 96% and 94% (0.241), 96% and 98% (0.252), and 94% and 100% (0.263), respectively. (c) Picture of the 96 multiwell plate containing 250 μL of positive (top panel) and negative (bottom panel) samples. The plate reading was carried out by a commercial multiwell reader that took less than 1 min.

number N of AuNPs on the virion surface is highly nonlinear (Figure S4b). The maximum number of AuNPs that can be placed on a perfectly spherical surface with 100 nm diameter is $N = 80$, but the steric hindrance offered by surface proteins like the spike one surely limits the filling capacity of the virion surface. In fact, from Figure S4b we see that the experimental value of $\lambda_{LSPR} = 560$ nm is achieved when $N = 70$, a value only slightly smaller than the maximum achievable. The extinction spectrum corresponding to $N = 70$ AuNPs (scaled to the experimental one) is reported in Figure 1c (golden continuous line) and shows a more than satisfactory agreement with the experimental one (red continuous line), thereby confirming that the simple model proposed here is able to capture the essential physical processes underlying the virion detection.

In order to test the validity of the colorimetric biosensor, we analyzed real samples previously examined by real-time PCR. The samples were from 45 positive to SARS-CoV-2 patients for which $C_t \leq 35$ and 49 negative patients ($C_t > 35$). For all of them, we measured the optical density at 560 nm (OD_{560}) by a commercial microplate reader (Figure 2a). It is quite evident the correlation between the C_t value (reported on the top scale) of the positives (red circles) and OD_{560}, whereas all the negatives (identified by a progressive number in the bottom scale) are randomly distributed providing a "control" value of $OD_{560}^{neg} = 0.22 \pm 0.02$. Also shown in Figure 2a is a horizontal line at an OD_{560} value of 0.252, which makes clear the ability to discriminate positives from negatives offered by our colorimetric biosensor. In fact, with such a threshold we get 96% and 98% for sensitivity and specificity, respectively. This result is even more remarkable if we consider that $C_t > 30$ correspond to a very low viral load for which the infection aptitude is questioned. To this aim, it is important to notice that in the early phase of the infection, high viral loads are detected by real-time PCR in upper respiratory specimens with low C_t readouts ($C_t < 20$, with our assay). In the late phase of the infection, a dramatic drop in viral loads is observed with higher C_t readouts ($C_t > 30$ with our assay). Positive results with high C_t readouts pose a diagnostic challenge, since they do not necessarily indicate active infection by a replicating virus. It has been observed using viral culture that patients with high C_t real-time PCR and protracted positivity are not infectious, suggesting that the assay likely detects non-active viral particles such as genetic material present in remnants of inactive virus,[35] thereby making our approach of high diagnostic value.

The receiver operating characteristic (ROC) curve from the data shown in Figure 2a is reported in Figure 2b together with the indication of three threshold values, all of them leading to sensitivity and specificity significantly higher than 90%. In particular, the highest threshold value (0.263) leads to 100% specificity while keeping the sensitivity at the remarkable value 94%. Overall, the high performance of the test associated with the colorimetric biosensor is demonstrated by the area under the ROC curve whose value is 0.98. The qualitative difference in the color between positives and negatives can be observed in Figure 2c that shows a picture of the multiwells containing the samples whose analysis is summarized in Figure 2a,b.

To measure the dose−response curve of the biosensor, we assessed the optical density OD_{560} of samples obtained by serial dilutions (1:10) of an initial volume with very high viral load ($C_t = 7$). The results are shown in Figure 3, in which OD_{560} is reported as a function of the relative concentration of SARS-CoV-2. For convenience, the top scale reports the equivalent C_t obtained by considering that 1:10 dilution corresponds to $\log_2 10 \approx 3.32$ change in C_t, whereas the vertical dashed blue line identifies the starting concentration. As it turns out, a detectable signal can be appreciated even after 7 serial dilutions ($1{:}10^7$) confirming the wide detection range resulting from the validation measurements reported in Figure 2.

The behavior of the OD_{560} as a function of the virion concentration C reported in Figure 3 can be described by the three-parameter Hill equation[36]

$$OD_{560}(C) = \frac{\Delta(OD_{560}) \cdot C^n}{K^n + C^n} + OD_{560}(0) \quad (1)$$

In eq 1, $OD_{560}(0) = OD_{560}^{neg} = 0.22$ is the OD of the "control" as deduced from the negative samples, $\Delta(OD_{560})$ is the maximum OD_{560} variation, K is the concentration (in this case it is a relative concentration) at which the OD_{560} variation reaches 50% of its maximum. and n is the so-called Hill's

https://dx.doi.org/10.1021/acssensors.0c01742
ACS Sens. XXXX, XXX, XXX−XXX

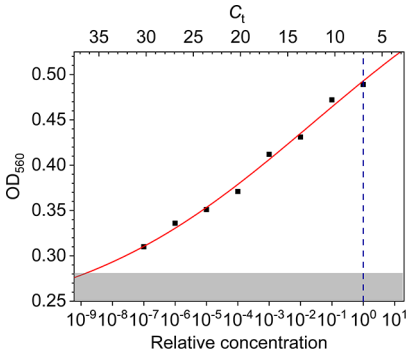

Figure 3. Optical density of the solution measured at 560 nm as a function of SARS-CoV-2 concentration (bottom axis). The virion concentration was obtained by serial dilution starting from a threshold cycle value C_t = 7 (vertical dashed blue line). Each decrease by a decade in virion concentration (bottom axis) corresponds to an increase of the nominal C_t of approximately 3.32 (top axis). The red continuous line is the best fit of the experimental data by the Hill equation. The uncertainty in the reading is taken as the resolution of the instrument, and the error bar is within the data point. The shaded area corresponds to values smaller than OD_{560} = 0.28, which is 3 standard deviations from the mean value of the negative controls.

coefficient.[37] The best fit of the experimental data with eq 1 yielded the curve in Figure 3 and the following values for the parameters: $\Delta(OD_{560}) = 0.45 \pm 0.11$, $K = 0.03 \pm 0.11$, and $n = 0.11 \pm 0.02$.

The (relative) concentration K is essentially undetermined as a consequence of the high detection range of our method, which entails small response to the concentration changes (low sensitivity) and, hence, high uncertainty on the concentration measurements. A value for n significantly smaller than 1 indicates the occurrence of a negatively cooperative binding, a behavior which we expect by considering that the probability a f-AuNP binds the virion reduces as the surface covering grows. Eventually, $\Delta(OD_{560})$ is the range of optical densities spanned by the biosensor. The shaded area in Figure 3 contains the values of OD_{560} within 3 standard deviation (SD) from the mean value of the control (OD_{560}^{neg} + 3SD = 0.28). Thus, according to 3SD criterion, we obtain C_t = 36.5 as the limit of detection of the biosensor in terms of real-time PCR cycle threshold. Thus, although real-time PCR sensitivity is hard to surpass, in the context of COVID-19 pandemic in which the detection of SARS-CoV-2 is required in nasopharyngeal swabs, our method is an efficient alternative when quick and widespread response cannot be provided by standard laboratory methods.

In conclusion, we realized a colorimetric biosensor based on a colloidal solution of AuNPs (20 nm, OD ≈ 1), each of them functionalized with Abs against one of the three surface proteins of SARS-CoV-2 (spike, envelope, and membrane). The ratio among the three kinds of functionalized AuNPs was 1:1:1. Although both the ratio and the size of AuNPs are still susceptible to optimization to allow one to push even further the limit of detection, the current performances of the biosensor would already permit its use as a test for mass screening, since the detection is based on the interaction among the virions and the pAb-functionalized AuNPs (single step detection) without any pretreatment (e.g., RNA extraction and amplification). The comparison of the readout of our biosensor at 560 nm with the threshold cycle (C_t) of a real-time PCR proved that viral loads corresponding to C_t = 36.5 are detected by the colorimetric biosensor. This threshold is of particular importance because it corresponds to a very low viral load for which the infecting capacity is likely negligible.[35] Such a good performance has to be ascribed to a high filling ratio of the virion surface that results from the presence of multiple Abs (three proteins are targeted) and an effective AuNP surface functionalization procedure (PIT). In fact, through PIT not only is one Fab always exposed to make AuNP highly "reactive", but also the Abs are attached to the surface (side-on position) without any linker (e.g., protein A), the latter being detrimental for the plasmonic interactions among AuNPs on which the colorimetric biosensor is based.

Another remarkable feature of the biosensor described here relies on its sensitivity to the virion rather than to its content (RNA). The importance of this is twofold: (1) after the calibration of the optical response, the biosensor lends itself as a powerful tool to quantify the viral load, a nontrivial issue in diagnostic assays in virology; (2) being sensitive only to the virions, the biosensor detects the presence of active viral particles; thus, our method is apt to assess the actual degree of infectiveness of a specimen.

As a final remark, we point out that the colorimetric solution described here can be easily modified to target other viruses. Thus, we expect that single-step colorimetric detection of viruses can become a general technique to be used for laboratory applications as well as point-of-care testing.

■ ASSOCIATED CONTENT

Supporting Information

The Supporting Information is available free of charge at https://pubs.acs.org/doi/10.1021/acssensors.0c01742.

Materials (S1). Instruments (S2). Gold nanoparticle synthesis (S3). Optical and morphological AuNP characterization (S4). Functionalization (S5). Storage of the samples and validation of the measurements with PCR (S6). Threshold cycle in PCR measurement and viral load (S7). FDTD optical simulations (S8). (PDF)

■ AUTHOR INFORMATION

Corresponding Authors

Giuseppe Portella − *Dipartimento di Scienze Mediche Traslazionali, Università di Napoli Federico II, 80131 Napoli, Italy*; Email: portella@unina.it

Raffaele Velotta − *Dipartimento di Fisica Ettore Pancini, Università di Napoli Federico II, 80126 Napoli, Italy*; orcid.org/0000-0003-1077-8353; Email: rvelotta@unina.it

Authors

Bartolomeo Della Ventura − *Dipartimento di Fisica Ettore Pancini, Università di Napoli Federico II, 80126 Napoli, Italy*

Michele Cennamo − *Dipartimento di Scienze Mediche Traslazionali, Università di Napoli Federico II, 80131 Napoli, Italy*

Antonio Minopoli − *Dipartimento di Fisica Ettore Pancini, Università di Napoli Federico II, 80126 Napoli, Italy*

Raffaele Campanile − *Dipartimento di Fisica Ettore Pancini, Università di Napoli Federico II, 80126 Napoli, Italy*

Sergio Bolletti Censi − *Cosvitec scarl, 80142 Napoli, Italy*

Daniela Terracciano − *Dipartimento di Scienze Mediche Traslazionali, Università di Napoli Federico II, 80131 Napoli, Italy*

https://dx.doi.org/10.1021/acssensors.0c01742
ACS Sens. XXXX, XXX, XXX−XXX

Complete contact information is available at:
https://pubs.acs.org/10.1021/acssensors.0c01742

Author Contributions

B.DV. and R.V. conceived of the biosensor. M.C., D.T., and G.P. carried out the real-time PCR measurements. B.DV. and M.C. measured the optical response of the biosensor. B.DV., A.M., G.P., and R.V. performed the data interpretation. R.C., S.BC., and D.T. carried out statistical analysis. A.M. and R.C. worked out the numerical simulations. A.M. and R.V. wrote the manuscript. D.T. and G.P. revised the manuscript.

Notes

The authors declare no competing financial interest.

■ ACKNOWLEDGMENTS

We thank Dr. Luigi Atripaldi, Dr. Roberto Parrella, and Dr. Claudia Tiberio for their availability to carry out preliminary tests in the Laboratory of Microbiology at Hospital "Domenico Cotugno" in Naples.

■ REFERENCES

(1) Guglielmi, G. The Explosion of New Coronavirus Tests That Could Help to End the Pandemic. *Nature* **2020**, *583* (7817), 506−509.
(2) Bustin, S. A.; Mueller, R. Real-Time Reverse Transcription PCR (QRT-PCR) and Its Potential Use in Clinical Diagnosis. *Clin. Sci.* **2005**, *109* (4), 365−379.
(3) Olofsson, S.; Brittain-Long, R.; Andersson, L. M.; Westin, J.; Lindh, M. PCR for Detection of Respiratory Viruses: Seasonal Variations of Virus Infections. *Expert Rev. Anti-Infect. Ther.* **2011**, *9* (8), 615−626.
(4) Appak, Ö.; Duman, M.; Belet, N.; Sayiner, A. A. Viral Respiratory Infections Diagnosed by Multiplex Polymerase Chain Reaction in Pediatric Patients. *J. Med. Virol.* **2019**, *91* (5), 731−737.
(5) Li, Z.; Yi, Y.; Luo, X.; Xiong, N.; Liu, Y.; Li, S.; Sun, R.; Wang, Y.; Hu, B.; Chen, W.; et al. Development and Clinical Application of A Rapid IgM-IgG Combined Antibody Test for SARS-CoV-2 Infection Diagnosis. *J. Med. Virol.* **2020**, *92*, 1518.
(6) Satyanarayana, M. Shortage of RNA Extraction Kits Hampers Efforts to Ramp up COVID-19 Coronavirus Testing. *Chem. Eng. News* 19 March, **2020**.
(7) Esbin, M. N.; Whitney, O. N.; Chong, S.; Maurer, A.; Darzacq, X.; Tjian, R. Overcoming the Bottleneck to Widespread Testing: A Rapid Review of Nucleic Acid Testing Approaches for COVID-19 Detection. *RNA* **2020**, *26* (7), 771−783.
(8) Pokhrel, P.; Hu, C.; Mao, H. Detecting the Coronavirus (COVID-19). *ACS Sensors* **2020**, *5*, 2283.
(9) Wen, T.; Huang, C.; Shi, F. J.; Zeng, X. Y.; Lu, T.; Ding, S. N.; Jiao, Y. J. Development of a Lateral Flow Immunoassay Strip for Rapid Detection of IgG Antibody against SARS-CoV-2 Virus. *Analyst* **2020**, *145*, 5345.
(10) Baker, A. N.; Richards, S.-J.; Guy, C. S.; Congdon, T. R.; Hasan, M.; Zwetsloot, A. J.; straube, A.; Walker, M.; Chessa, S.; Pergolizzi, G. The SARS-COV-2 Spike Protein Binds Sialic Acids, and Enables Rapid Detection in a Lateral Flow Point of Care Diagnostic Device. *ACS Cent. Sci.* **2020**, 1.
(11) Montesinos, I.; Gruson, D.; Kabamba, B.; Dahma, H.; Van den Wijngaert, S.; Reza, S.; Carbone, V.; Vandenberg, O.; Gulbis, B.; Wolff, F. Evaluation of Two Automated and Three Rapid Lateral Flow Immunoassays for the Detection of Anti-SARS-CoV-2 Antibodies. *J. Clin. Virol.* **2020**, *128*, 104413.
(12) Sheridan, C. Fast, Portable Tests Come Online to Curb Coronavirus Pandemic. *Nat. Biotechnol.* **2020**, *38* (5), 515−518.
(13) Lassaunière, R.; Frische, A.; Harboe, Z. B.; Nielsen, A. C.; Fomsgaard, A.; Krogfelt, K. A.; Jørgensen, C. S. Evaluation of Nine Commercial SARS-CoV-2 Immunoassays. *medRxiv* **2020**, 1 DOI: 10.1101/2020.04.09.20056325.
(14) Tromberg, B. J.; Schwetz, T. A.; Pérez-Stable, E. J.; Hodes, R. J.; Woychik, R. P.; Bright, R. A.; Fleurence, R. L.; Collins, F. S. Rapid Scaling Up of Covid-19 Diagnostic Testing in the United States — The NIH RADx Initiative. *N. Engl. J. Med.* **2020**, *383*, 1071.
(15) Tang, L.; Li, J. Plasmon-Based Colorimetric Nanosensors for Ultrasensitive Molecular Diagnostics. *ACS Sensors* **2017**, *2* (7), 857−875.
(16) Chaudhary, A.; Khan, S.; Gupta, A.; Nandi, C. K. Effect of Surface Chemistry and Morphology of Gold Nanoparticle on the Structure and Activity of Common Blood Proteins†. *New J. Chem.* **2016**, *40*, 4879−4883.
(17) Chen, Y.; Ming, H. Review of Surface Plasmon Resonance and Localized Surface Plasmon Resonance Sensor. *Photonic Sens.* **2012**, *2* (1), 37−49.
(18) Amendola, V.; Pilot, R.; Frasconi, M.; Maragò, O. M.; Iatì, M. A. Surface Plasmon Resonance in Gold Nanoparticles: A Review. *J. Phys.: Condens. Matter* **2017**, *29* (20), 203002.
(19) Li, M.; Cushing, S. K.; Wu, N. Plasmon-Enhanced Optical Sensors: A Review. *Analyst* **2015**, *140* (2), 386−406.
(20) Jazayeri, M. H.; Amani, H.; Pourfatollah, A. A.; Pazoki-Toroudi, H.; Sedighimoghaddam, B. Various Methods of Gold Nanoparticles (GNPs) Conjugation to Antibodies. *Sens. Bio-Sensing Res.* **2016**, *9*, 17−22.
(21) Della Ventura, B.; Schiavo, L.; Altucci, C.; Esposito, R.; Velotta, R. Light Assisted Antibody Immobilization for Bio-Sensing. *Biomed. Opt. Express* **2011**, *2* (11), 3223−3231.
(22) Della Ventura, B.; Banchelli, M.; Funari, R.; Illiano, A.; De Angelis, M.; Taroni, P.; Amoresano, A.; Matteini, P.; Velotta, R. Biosensor Surface Functionalization by a Simple Photochemical Immobilization of Antibodies: Experimental Characterization by Mass Spectrometry and Surface Enhanced Raman Spectroscopy. *Analyst* **2019**, *144* (23), 6871−6880.
(23) Funari, R.; Della Ventura, B.; Schiavo, L.; Esposito, R.; Altucci, C.; Velotta, R. Detection of Parathion Pesticide by Quartz Crystal Microbalance Functionalized with UV-Activated Antibodies. *Anal. Chem.* **2013**, *85* (13), 6392−6397.
(24) Funari, R.; Terracciano, I.; Della Ventura, B.; Ricci, S.; Cardi, T.; D'Agostino, N.; Velotta, R. Label-Free Detection of Gliadin in Food by Quartz Crystal Microbalance-Based Immunosensor. *J. Agric. Food Chem.* **2017**, *65* (6), 1281−1289.
(25) Fulgione, A.; Cimafonte, M.; Della Ventura, B.; Iannaccone, M.; Ambrosino, C.; Capuano, F.; Proroga, Y. T. R.; Velotta, R.; Capparelli, R. QCM-Based Immunosensor for Rapid Detection of Salmonella Typhimurium in Food. *Sci. Rep.* **2018**, *8* (1), 16137.
(26) Cimafonte, M.; Fulgione, A.; Gaglione, R.; Papaianni, M.; Capparelli, R.; Arciello, A.; Bolletti Censi, S.; Borriello, G.; Velotta, R.; Della Ventura, B. Screen Printed Based Impedimetric Immunosensor for Rapid Detection of Escherichia Coli in Drinking Water. *Sensors* **2020**, *20* (1), 274.
(27) Della Ventura, B.; Iannaccone, M.; Funari, R.; Pica Ciamarra, M.; Altucci, C.; Capparelli, R.; Roperto, S.; Velotta, R. Effective Antibodies Immobilization and Functionalized Nanoparticles in a Quartz-Crystal Microbalance-Based Immunosensor for the Detection of Parathion. *PLoS One* **2017**, *12* (2), No. e0171754.
(28) Iarossi, M.; Schiattarella, C.; Rea, I.; De Stefano, L.; Fittipaldi, R.; Vecchione, A.; Velotta, R.; Della Ventura, B. Colorimetric Immunosensor by Aggregation of Photochemically Functionalized Gold Nanoparticles. *ACS Omega* **2018**, *3* (4), 3805−3812.
(29) Minopoli, A.; Sakač, N.; Lenyk, B.; Campanile, R.; Mayer, D.; Offenhäusser, A.; Velotta, R.; Della Ventura, B. LSPR-Based Colorimetric Immunosensor for Rapid and Sensitive 17β-Estradiol Detection in Tap Water. *Sens. Actuators, B* **2020**, *308*, 127699.
(30) Liu, Y.; Zhang, L.; Wei, W.; Zhao, H.; Zhou, Z.; Zhang, Y.; Liu, S. Colorimetric Detection of Influenza A Virus Using Antibody-Functionalized Gold Nanoparticles. *Analyst* **2015**, *140* (12), 3989−3995.
(31) Zhu, N.; Zhang, D.; Wang, W.; Li, X.; Yang, B.; Song, J.; Zhao, X.; Huang, B.; Shi, W.; Lu, R.; et al. A Novel Coronavirus from

Patients with Pneumonia in China, 2019. *N. Engl. J. Med.* **2020**, *382* (8), 727−733.
(32) Bar-On, Y. M.; Flamholz, A.; Phillips, R.; Milo, R. SARS-CoV-2 (COVID-19) by the Numbers. *eLife* **2020**, *9*, No. e57309.
(33) Ma, L.; Zhu, S.; Tian, Y.; Zhang, W.; Wang, S.; Chen, C.; Wu, L.; Yan, X. Label-Free Analysis of Single Viruses with a Resolution Comparable to That of Electron Microscopy and the Throughput of Flow Cytometry. *Angew. Chem., Int. Ed.* **2016**, *55* (35), 10239−10243.
(34) Haynes, W. M. *CRC Handbook of Chemistry and Physics*, Haynes, W. M.; Lide, D. R.; Bruno, T. J., Eds.; CRC Press, 2016. DOI: 10.1201/9781315380476.
(35) Motley, M. P.; Bennett-Guerrero, E.; Fries, B. C.; Spitzer, E. D. Review of Viral Testing (Polymerase Chain Reaction) and Antibody/Serology Testing for Severe Acute Respiratory Syndrome-Coronavirus-2 for the Intensivist. *Crit. care Explor.* **2020**, *2* (6), e0154−e0154.
(36) Goutelle, S.; Maurin, M.; Rougier, F.; Barbaut, X.; Bourguignon, L.; Ducher, M.; Maire, P. The Hill Equation: A Review of Its Capabilities in Pharmacological Modelling. *Fundam. Clin. Pharmacol.* **2008**, *22* (6), 633−648.
(37) Li, Y.; Wang, Y.; Huang, G.; Gao, J. Cooperativity Principles in Self-Assembled Nanomedicine. *Chem. Rev.* **2018**, *118*, 5359.

https://dx.doi.org/10.1021/acssensors.0c01742
ACS Sens. XXXX, XXX, XXX−XXX